Remelting by continuous feeding of rolled scrap into a melt

Snorre Farner[1], Frede Frisvold[2], and Thorvald Abel Engh[1]

[1] Department of Materials Technology and Electrochemistry, Norwegian University of Science and Technology N-7491 Trondheim, Norway, E-mail: farner@pvv.ntnu.no

[2] Ålesund College, N-6025 Ålesund, Norway

Abstract

Metal losses during remelting is common when recycling aluminium. Reduction of these losses could give a substantial economic gain. Experiments with continuous feeding of aluminium plates into molten aluminium have been performed. A simple steady-state mathematical model has been developed that gives the temperature profile and the penetration depth into the melt as a function of the feeding velocity, superheat, and the heat-transfer coefficients from melt to solid and from a solidified shell to the plate. A criterion for shell formation is also formulated.

The results can be applied to understand more complex systems where shredded scrap is fed into molten aluminium. The model presented could be of direct interest when feeding rolled scrap into molten aluminium.

1 Introduction

Recycling of aluminium is a growing industry. Partly this is due to an increasing environmental consciousness, but the potential profit is high due to its low energy demands compared with primary production [1] and low scrap price relative to the price of ingot. The challenges are many, and one of the major concerns is the amount of aluminium that is lost due to oxidation.

In many recycling plants, aluminium scrap is melted by charging into molten aluminium in a reverberatory furnace. Although solid aluminium has higher density than liquid aluminium, even compacted scrap tends to float on the melt surface. This can be attributed to air inevitably contained in the scrap and thereby lowering the bulk density. A strong oxide skin as well as solidification of melt between the outermost scrap pieces is believed to restrict liquid-aluminium flow in between the scrap pieces. A hot atmosphere, which always will contain oxygen, will pre-heat the scrap surfaces that are above the melt surface, and increase oxidation. The oxide skin on the scrap surfaces tends to envelop metallic aluminium when the scrap melts. Metallic aluminium not released from the oxide is skimmed off as dross. Thus, the dross contains large amounts of metallic aluminium which is only partly recovered during a following dross treatment. Floating scrap has been attempted submerged more or less successfully by stirring the melt, compacting the scrap, or pushing it under the melt surface in various ways. Pietsch [2] investigated rolling of swarf to compacted sheets in order to increase the density enough for easy submersion. We suggest rolling shredded scrap, feeding it directly into the melt, and thereby submerging it mechanically in one continuous movement.

In the current paper, we present experimental results and a mathematical model for a simplified system where feeding of a thin aluminium plate into an aluminium melt and the melting mechanism are investigated.

2 Previous work

The heat-transfer resistance between a solidifying melt and a cold metal surface has been studied at least since the 1960's. It has been found to depend on superheat, applied contact pressure, material properties, surface coatings, and more [3]. The heat-transfer coefficient h (the inverse of the heat-transfer resistance) for heat transfer from a solidifying melt in a cold mould shows an initial peak of 3 to above $10\,\mathrm{kW/m^2K}$ within the first minute of the casting and then decreases to a constant value about 10–20 % of this, ostensibly because the contact pressure of the metal against the mould decreases when the mould expands and the metal contracts as it solidifies [4–9]. If the mould material is immersed into a melt, h is observed to increase [10] since the

metal contracts around the expanding mould. Kim and Lee confirm this by solidifying the metal between two co-axial circular mould walls [11].

When a cold alloy addition is immersed in a melt, heat is extracted from the closest melt which then tends to solidify and form a shell around the addition. This has long been studied without considering a heat-transfer resistance between the shell and the addition (represented by the inner heat-transfer coefficient h_i). Only the convective heat-transfer coefficient of the melt [12,13] is considered. Already in 1980, Mucciardi [14] reported the existence of an inner heat-transfer resistance, but it seems to have been neglected in the literature until lately [15, 16]. The value of h_i varies between 1 and 6 $\mathrm{kW/m^2K}$ and has been measured to 4 and 2.5 $\mathrm{kW/m^2K}$ for aluminium additions in an aluminium melt by Røhmen [15] and Goudie and Argyropoulos [16], respectively. The latter authors performed a number of experiments with a variety of addition metals and several different melts, and correlated h_i with the ratio of the expansion coefficients of the addition and the melt. Although no reports of the time dependence of h_i have been found for additions in a melt, these authors made a similar conclusion that the heat transfer increases with increasing contact pressure of the shell against the addition.

Furthermore, Goudie and Argyropoulos [16] did also measure the shell temperature during immersion of aluminium in a tin melt with melting point at 232°C. They observed that, at 30°C superheat, the temperature remained close to the melting point except for a depression of about 30°C during the first 3 s of totally about 25 s of shell period.

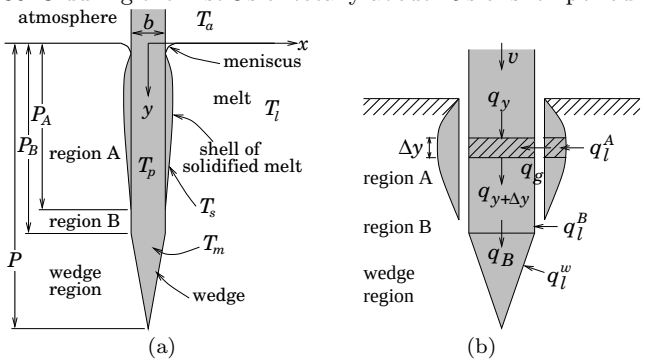

Fig. 1 Continuous feeding of a metal plate into a melt: (a) the system and dimensions, and (b) the heat flow.

3 Feeding of a thin plate into a melt

A metal plate ideally extending infinitely far upwards is fed vertically into a molten metal at a steady velocity (Figure 1a). After a transient period, the system is assumed to be in a steady state. Where the plate penetrates the melt surface, the oxide skin on the surface is pulled down and a meniscus is formed. In this area, heat starts to flow from the melt into the cold plate. If the supply of heat from the melt is lower than the heat flow into the plate, the melt closest to the plate solidifies and forms a shell on the plate. This is normally the case. As the plate moves downwards into the melt, the plate temperature increases, and the shell grows until the heat flow into and out of the shell balance each other. From this point on, the shell melts back and finally vanishes. Heat now flows directly from the melt to the plate, and after a distance the plate reaches its melting point and starts to melt. The model now assumes that the temperature remains at the melting point while the heat flow from the melt supplies the latent heat of melting. This final part is modelled as a wedge. The co-ordinate system and important quantities are shown in Figure 1a.

4 Experimental setup

4.1 Apparatus

A sketch of the experimental setup is shown in Figure 2a. The feeding apparatus consists of a roller for coiled aluminium plate and a feeding mechanism under it. The feeding mechanism is shown in Figure 2b and consists of two counter-rotating feeding rolls of which one is attached to a speed-controlled Faulhaber motor, and two rolls below which straighten out the plate before it continues down into the melt. The apparatus was placed on the top of a resistance-heated, 40-cm diameter crucible and shielded against radiation from the melt.

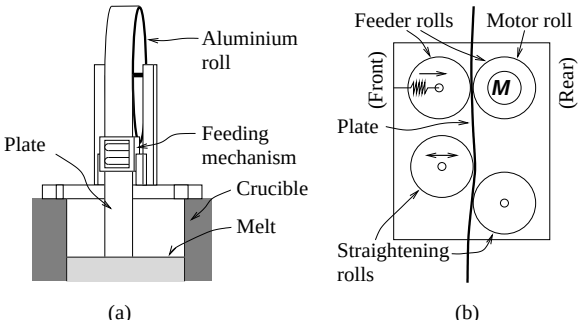

Fig. 2 Sketches of (a) the full experimental setup and (b) the feeding mechanism in particular

The crucible was filled with 100 kg of commercially pure aluminium melt (99.5 %, AA1050). The melt surface was 60 cm below the feeding mechanism. The melting point T_m of the melt was measured by slowly letting a small ladle of melt solidify and melt with two thin thermocouples continuously measuring the temperature. The flat level of the temperature occurred at about 660°C. The plate material was made of the same alloy and thus assumed to have the same melting point. It was rolled to 0.54 mm thickness, cut to a width of 10.0 cm, and delivered in coils of many metres length. The coils were not cleaned in particular, and remains of rolling oil could be seen at some places. One coil was cleaned with ethanol to see whether the oil had any important effect, but no difference could be detected within the experimental uncertainties.

Two thermocouples were immersed in the melt, one close to the crucible wall and one close to where the plate penetrates the melt surface. A few experiments were also performed with thermocouples between two plates. The thermocouples were point-welded to one of the plates 5 cm vertically apart. For these measurements, plates of 200 cm length were used of which 124 cm could be fed into the melt. The upper thermocouple was attached so that it was well immersed before the plate was pulled out of the melt.

4.2 Procedure

Several series of penetration experiments were performed. Before each series, the melt temperature T_l (measured by the melt thermocouple closest to the plate) was held constant at temperatures in the range 700 to 800°C. The oxide skin was skimmed off the melt surface before each run. A few runs were performed without skimming for comparison, but the penetration depth of these runs lined up well with the other ones. Thus, although the skin thickness may vary a little with melt temperature and the time between skimming and measurement, the variations can be considered as negligible within the experimental uncertainties.

The feeding motor was started at a given velocity v (6.4, 9.6, 12.8, or 16.0 cm/s), and the plate was fed for about 15 seconds including the distance down to the melt (60 cm). In order to retain the penetration depth of the plate and the shell, the motor was instantly reversed at full speed (about 65 cm/s) so that the plate was quickly withdrawn out of the melt. After cooling in air, the melted part was cut off for later analysis. During the feeding, the motor speed and the melt temperature T_l were measured ten times per second. In a few experiments, we also video-filmed the plate to be able to study it in slow motion.

95 runs were performed in series usually of eight runs, two at each velocity. The bath temperature fell 5°C at most within a series, and the melt temperature was changed between each series. Three runs were also performed with thicker plates (1.50 mm), one at 6.4 and two at 3.2 cm/s. For the measurements with thermocouples connected to the plate, only one feeding velocity, $v = 9.6$ cm/s, was used.

5 Mathematical model

In order to derive a simple semi-analytical mathematical model (see Figure 1b), several assumptions have been made:

1. A steady state is reached,
2. the material properties are constant,
3. the heat-transfer coefficients (h_g and h_l) are constant,
4. h_l from the bulk melt also accounts for the sensible heat released from the melt before solidification,
5. a high heat conduction inside the plate gives horizontal isotherms inside the plate,
6. the temperature in the plate at the penetration point ($y = 0$) is constant and equal to T_a,
7. the entire wedge is assumed to be constant at the melting point of the plate, and
8. the shell is considered to have constant temperature equal to its melting point.

The last assumption is justified by the shell-temperature measurements reported by Goudie and Argyropoulos [16] (see end of Section 2). Note that the plate and melt are of the same alloy so that the plate and the shell have the same melting point.

The mathematical model consists of four connected heat equations: one equation for each of the two regions A and B of the plate, one for the shell formed outside region A, and the last for the wedge.

In the plate, the heat balance of a horizontal cross section of thickness Δy (see Figure 1b) is governed by the vertical convective and conductive heat flow q_y at the distance y below the surface, and the heat flow q_g from the shell over a gap between the shell and the plate. The heat flow over the gap can be expressed by Newton's law of cooling as proportional to the temperature difference over the gap and the heat-transfer coefficient h_g: $q_g = h_g(T_m - T_p)$. The resulting balance for the cross section is

$$-\Delta\left(-kb\frac{dT_p}{dy} + \rho c v b T_p\right) + 2h_g(T_m - T_p)\Delta y = 0. \quad (1)$$

The nomenclature section at the end of the paper gives the meaning of the symbols. Dividing Equation (1) by Δy, letting this approach zero, and introducing the dimensionless quantities defined in the nomenclature section, we obtain the temperature profile along the plate in region A, with prime denoting derivative with respect to η:

$$\theta_p'' - Pe\,\theta_p' - 2Bi\,(\theta_p - 1) = 0, \quad 0 \le \eta < \Pi_A. \quad (2)$$

In region B, where the shell has vanished, the heat flows directly from the melt into the plate with no gap resistance. We replace h_g with the heat-transfer coefficient h_l through the melt boundary layer, and T_m with T_l:

$$\theta_p'' - Pe\,\theta_p' - 2Nu\,(\theta_p - \theta_l) = 0, \quad \Pi_A \le \eta < \Pi_B. \quad (3)$$

The general solutions to the plate-temperature equations (2) and (3) are

$$\begin{aligned} \theta_p(\eta) &= 1 + Ae^{\lambda_1\eta} + Be^{-\lambda_2\eta}, & 0 \le \eta < \Pi_A, \\ \theta_p(\eta) &= \theta_l + A'e^{\lambda_1'\eta} + B'e^{-\lambda_2'\eta}, & \Pi_A \le \eta < \Pi_B, \end{aligned} \quad (4)$$

where

$$\begin{aligned} \lambda_1 &= \tfrac{1}{2}Pe\left(\sqrt{1 + \tfrac{8Bi}{Pe^2}} + 1\right), \\ \lambda_2 &= \tfrac{1}{2}Pe\left(\sqrt{1 + \tfrac{8Bi}{Pe^2}} - 1\right). \end{aligned} \quad (5)$$

The constants A, B, A', and B' are to be determined by the boundary conditions. To obtain λ_1' and λ_2', Bi is replaced with Nu.

The heat balance for a cross section of the shell is reduced to a one-dimensional problem of the shell thickness due to the assumption of constant temperature. The heat flow from the melt is $q_l^A = h_l(T_l - T_m)$ and differs from q_g into the plate by the latent heat of solidification or melting:

$$q_l^A\sqrt{1 + \left(\frac{dx_s}{dy}\right)^2} - q_g + \rho v L\frac{dx_s}{dy} = 0, \quad (6)$$

where the square root appears because the outer surface of the shell curves and thereby slightly increases the surface area through which the heat flows. Equation (6) is easily solved with respect to dx_s/dy, and the sign of the resulting square root is chosen such that $q_g = q_l^A$ when $dx_s/dy = 0$. We rewrite it for convenience with dimensionless quantities:

$$\frac{d\xi_s}{d\eta} = \frac{Bi\,(1 - \theta_p)}{Pe\,Sf}\times \quad (7)$$
$$\times\frac{1 - \sqrt{1 + \left[1 - \left(\frac{Nu\,(\theta_l - 1)}{Pe\,Sf}\right)^2\right]\left[\left(\frac{Nu\,(\theta_l - 1)}{Bi\,(1 - \theta_p)}\right)^2 - 1\right]}}{1 - \left(\frac{Nu\,(\theta_l - 1)}{Pe\,Sf}\right)^2}.$$

Finally, the heat flowing into the wedge from the melt ought to balance the latent heat of melting of the plate material convected from region B and the heat conduction $q_B = -k\,dT_p/dy$ into this region. As a consequence of a constant wedge temperature, there are no heat gradients in the wedge, and we cannot allow any heat conduction through the wedge or out of it. This leaves $q_B = 0$. The steady-state heat balance for the wedge becomes

$$q_l^w \sqrt{1 + \left(\frac{2(P - P_B)}{b}\right)^2} = -q_B + \rho v L, \tag{8}$$

where $P - P_B$ is the vertical length of the wedge (see Figure 1a) and $q_l^w = h_l(T_l - T_m)$. The dimensionless form is

$$\Pi - \Pi_B = \frac{1}{2}\sqrt{\left(\frac{Pe\,Sf}{Nu(\theta_1 - 1)}\right)^2 - 1}. \tag{9}$$

We now have six unknown constants A, B, A', B', Π_A, and Π_B. The dimensionless penetration depth Π_A of the shell is determined by integrating Equation (7) numerically and finding its root. The rest of the constants are determined with the aid of five boundary conditions. Four of them demand continuous temperature and derivative of this between the three regions of the plate. In particular, the two conditions connecting region B and the wedge, become $\theta_p(\eta) = 1$ and $\theta_p'(\eta) = 0$ when $\eta = \Pi_B$, and the last boundary condition gives the starting temperature of the plate at the penetration point: $\theta_p(\eta) = 0$ when $\eta = 0$. The penetration depths Π_A and Π_B of region A and B, respectively, end up as implicitly given constants while the remaining four constants are easily solved explicitly, although too long and laborious to reproduce in this paper. Example plots are presented in Section 7.

6 Criterion for shell formation

The heat drawn into the plate upon immersion is taken from the immediately surrounding melt. This heat flow is restricted by an inner heat-transfer resistance through the melt/plate interface, which might consist of paint or a gas film in addition to a phase-boundary resistance. The heat transport to this surrounding melt from the bulk melt is similarly limited by an outer heat-transfer resistance through the melt boundary layer. If the heat supply from the bulk melt is lower than the heat drawn into the plate, the immediately surrounding melt solidifies and a shell is formed. Once a shell is established, the heat-transfer resistances may change due to the gap that is formed between the shell and the plate. Shell formation thus requires that the heat flow q_l from the bulk melt must be less than the heat flow q_g over the gap into the plate. This is valid when the heat conduction inside the shell is so good that the heat-flow resistance through the shell is negligible (assumption 8). Mathematically, the criterion for shell formation is

$$h_l(T_l - T_m) < h_g(T_m - T_a) \tag{10}$$

where T_a is the initial temperature of the plate. In dimensionless form we obtain that

$$\theta_l - 1 < \frac{Bi}{Nu} \qquad \text{gives shell formation.} \tag{11}$$

This falls directly out of Equation (7) when the initial shell growth $d\xi_s/d\eta$ at $\eta = 0$ is greater than zero.

We can thus inhibit shell formation by increasing either the dimensionless superheat, the heat transfer from the melt, or the gap resistance between the shell and the plate. The latter does not seem to be a good idea as it will increase the melting time as well. Increasing the heat transfer from the melt is an option as it can be attained by stirring. The dimensionless superheat can be increased by increasing the melt temperature, but also by pre-heating the plate.

7 Results and discussion

Figure 3 shows two plates after immersion and quick withdrawal from the melt. To the left, a typical plate with shell is shown. On the edges of the plate, it can be seen that the solidified melt reaches higher than on the front surface. This can be explained by noting that no significant meniscus was observed on the edges. The shell height on the edges was thus considered the best way to measure the penetration point just before withdrawal.

The right plate in Figure 3 is a representative example of a plate without a solidified shell. Also in these cases there is an edge shell, which defines the penetration point. Other heat-transfer conditions on the thin edge surface seems to be a natural reason for this.

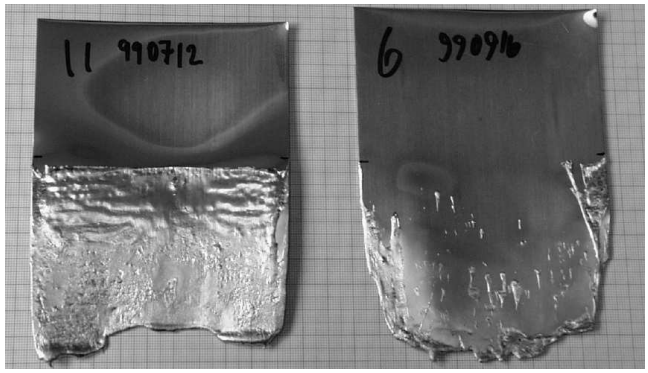

Fig. 3 Photograph of typical immersed plates, with (left) and without (right) shell.

Often, it was difficult to determine the borders between the three regions because of a thick oxide skin covering the immersed plate. Thus the total penetration depth alone was used for fitting the model to the measured values. The penetration depth was established by taking the average of the penetration depth at five positions along the plate width: symmetrically 1 and 3 cm from the edges and the last at the centre of the plate. It could vary with up to a fifth of the depth, probably because of the oxide skin making a drop-like edge as seen in Figure 3. The standard deviation was calculated and used as weights in the curve fitting. The fitting parameters were the two heat-transfer coefficients, and all measurements with thin plates ($b = 0.54$ mm) were used; at all four feeding velocities and all melt temperatures.

The heat-transfer coefficients became $h_g = 4.4\,\mathrm{kW/m^2K}$ ($Bi = 0.0107$) and $h_l = 21.6\,\mathrm{kW/m^2K}$ ($Nu = 0.052$), and the fitted curves and the experimental penetration depths are

shown in Figures 4 and 5 with dimensionless quantities, as defined in the nomenclature section. The gap heat-transfer coefficient h_g is well within what is previously reported.

The following material properties were used: $T_m = 660^\circ\mathrm{C}$, $L = 396\,\mathrm{kJ/kg}$, $k = 224\,\mathrm{W/mK}$, $c = 1200\,\mathrm{J/kg\,K}$, and $\rho = 2700\,\mathrm{kg/m^3}$. The ambient temperature (the initial plate temperature) was assumed to be $T_a = 20^\circ\mathrm{C}$. Curve fitting with $T_a = 40^\circ\mathrm{C}$ gave insignificant deviation in Bi and Nu. The penetration depths for the thicker plates and the double plate with thermocouples are shown in Figure 6.

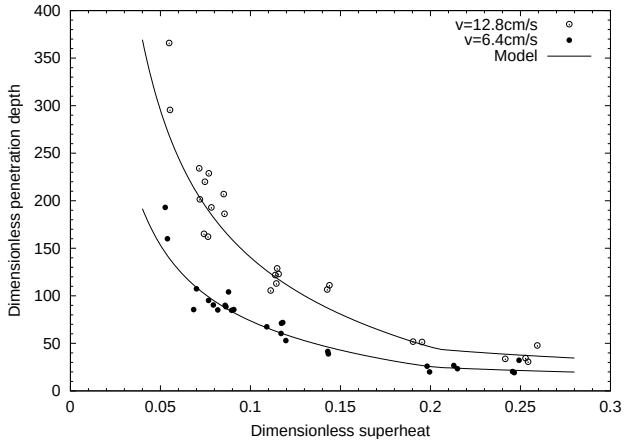

Fig. 4 The penetration depth $\Pi = P/b$ versus superheat $\theta_l = (T_l - T_a)/(T_m - T_a)$ at velocities $v = 6.4$ and $14.8\,\mathrm{cm/s}$.

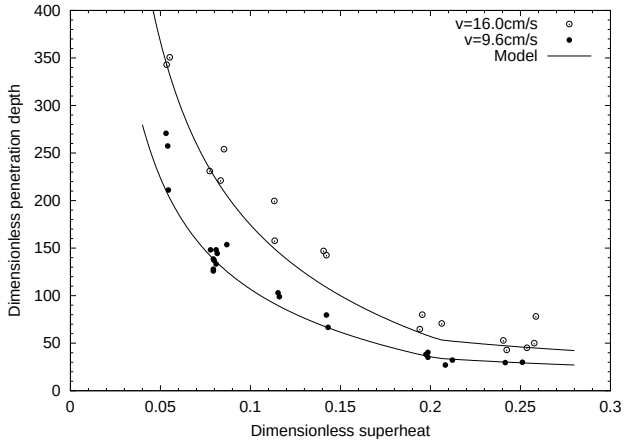

Fig. 5 The penetration depth $\Pi = P/b$ versus superheat $\theta_l = (T_l - T_a)/(T_m - T_a)$ at velocities $v = 9.6$ and $16.0\,\mathrm{cm/s}$.

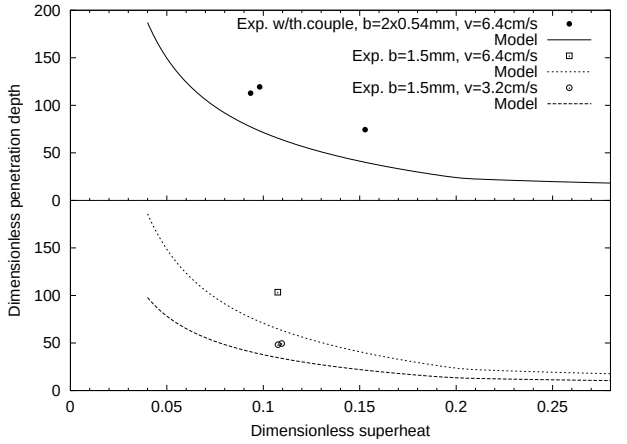

Fig. 6 The penetration depth $\Pi = P/b$ versus superheat $\theta_l = (T_l - T_a)/(T_m - T_a)$ for thicker plates ($b = 1.50\,\mathrm{mm}$) and double thin plates with thermocouple at velocity $v = 3.2$ and $6.4\,\mathrm{cm/s}$.

For the thin plates, the penetration depth was quite easily correlated to feeding velocity and superheat even though h_l was presumed independent of the feeding velocity. But for the thicker plates and the double plates, the penetration depth was larger than calculated with the obtained heat-transfer coefficients, which are not expected to change with plate thickness. This disagreement is probably due to the assumption that the plate had to be thin in order to yield approximately horizontal isotherms. The heat needs more time to enter the centre of thicker plates, and the isotherms will be curved like U's, also in the wedge region. Slower heating and melting of the plate and thereby a larger penetration depth is expected. It should however be noted that the discrepancy is roughly the same for double and almost triple thickness, so more experiments with thick plates are required to quantify the deviation.

Figure 7 shows measured and calculated temperature profiles and calculated shell thickness for one of the double-plate measurements with thermocouples. The measurement must be considered as preliminary, but is included for completeness. In the figure, the horizontal axis ends at the measured penetration depth for the plate, and similarly the calculated temperature ends at the theoretical penetration depth. Measurement time was transformed to dimensionless penetration distance by multiplying with v/b, and its zero point was set at the point where the temperature started to increase. T_1 is the temperature of the upper thermocouple which was the last one to enter the melt. Of course only the temperature points measured before the plate was withdrawn, are shown.

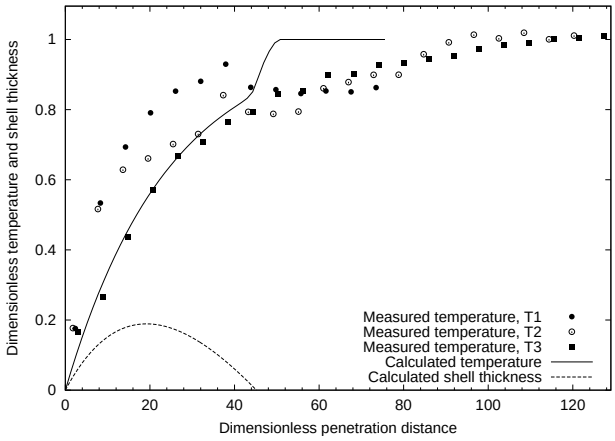

Fig. 7 The measured temperature profile of a sandwich of two thin plates ($b = 2 \times 0.54\,\mathrm{mm}$) with a thermocouple between compared with a theoretical curve for $b = 1.08\,\mathrm{mm}$.

With the attained values of the heat-transfer coefficients, the criterion for shell formation should be $\theta_l < 1.206$, i.e. $T_l \simeq 792^\circ\mathrm{C}$. This is seen as a break in the curve at this temperature in Figures 4 to 6. By pre-heating the plate to $300^\circ\mathrm{C}$, which should only give a negligible increase in oxidation, the melt temperature need not be higher than about

734°C, provided, of course, that the heat-transfer coefficients do not vary with the superheat. Absence of shell was observed in several cases below this limit, but mostly on one side only. Above the limit, shell growth was rather frequent, although only a very few had a shell on both sides. Thus, it is obvious that other important mechanisms control shell formation as well.

8 Conclusions

A simple one-dimensional mathematical model of melting of thin metal plates (a model of rolled scrap) has been developed and compared with experiments. The mathematical model gives the penetration depth and temperature profile down along the plate. For plates of uniform thickness, the fit was good, but it seems to deviate when plate thickness is increased.

A criterion is presented for when a solidified shell is not formed.

Probably, to describe systems when a thick plate such as rolled scrap is added, numerical methods must be employed. The present model can be used as a reference for such calculations.

9 Further work

Experiments with painted (lacquered) plates should be carried out to vary the inner heat-transfer coefficient h_g. The flow conditions should also be varied and the feeding velocity be considered in predicting and fitting the melt-to-shell heat-transfer coefficient h_l. Heat flow upwards in the plate above the melt as well as how the meniscus affects heat transfer from the melt should be taken into account. This will be dealt with in a doctor thesis soon to be submitted [17].

Acknowledgements: Hydro Aluminium Holmestrand Rolling Mill AS and the Norwegian Research Council are gratefully acknowledged for financial support, and the former also for providing the materials used.

Nomenclature

	Description	Dimensionless
b	Plate thickness	1
c	Specific heat of solid (J/kg K)	
h_g	Gap heat-transfer coeff. (W/m^{2}K)	$Bi = h_g b/k$
h_l	Heat-transfer coeff. in liquid (W/m^{2}K)	$Nu = h_l b/k$
k	Thermal conductivity of solid (W/mK)	
L	Latent heat (J/kg)	$Sf = \frac{L}{c(T_m - T_a)}$
P_A	Penetration depth of region A (m)	$\Pi_A = P_A/b$
P_B	Penetration depth of region B (m)	$\Pi_B = P_B/b$
P	Total penetration depth (m)	$\Pi = P/b$
q	Heat flow (W/m^2)	
ρ	Density of solid (kg/m^3)	
T_p	Plate temperature (K,°C)	$\theta_p = \frac{T_p - T_a}{T_m - T_a}$
T_m	Melting point (K,°C)	$\theta_m = 1$
T_l	Liquid-metal temperature (K,°C)	θ_l (see θ_p)
T_a	Ambient/initial plate temperature (K,°C)	$\theta_a = 0$
v	Feeding velocity (m/s)	$Pe = \rho c v b/k$
x_s	Shell thickness (m)	$\xi_s = x_s/b$
y	Vertical co-ordinate (m)	$\eta = y/b$

References

[1] H. A. Øye et al., Aluminum: Approaching the new millennium, *JOM*, (1999), pp. 29–42.

[2] W. Pietsch, Briquetting of aluminum swarf for recycling, in *Light Metals 1993*, Ed.: S. K. Das, TMS, 1993, pp. 1045–1051.

[3] W. D. Griffith, The heat-transfer coefficient during the unidirectional solidification of an Al–Si alloy casting, *Metallurgical and Materials Transactions B*, **30** (1999), pp. 473–482.

[4] K. Ho and R. D. Pehlke, Metal-mold interfacial heat transfer, *Metallurgical Transactions B*, **16** (1985), pp. 585–594.

[5] Y. Nishida, W. Droste, and S. Engler, The air-gap formation process at the casting-mold interface and the heat transfer mechanism through the gap, *Metallurgical Transactions B*, **17** (1986), pp. 833–844.

[6] G. Fortin, P. R. Louchez, and F. H. Samuel, Evolution of the heat transfer during the radial solidification of pure aluminium, *La Revue de Métallurgie*, **91** (1994), pp. 771–780 (in French).

[7] R. W. Lewis and R. S. Ransing, A correlation to describe interfacial heat transfer during solidification simulation and its use in the optimal feeding design of castings, *Metallurgical and Materials Transactions B*, **29** (1998), pp. 437–448.

[8] F. Lau, W. B. Lee, S. M. Xiong, and B. C. Liu, A study of the interfacial heat transfer between an iron casting and a metallic mould, *Journal of Materials Processing Technology*, **79** (1998), pp. 25–29.

[9] T. Loulou, E. A. Artyukhin, and J. P. Bardon, Estimation of thermal contract resistance during the first stages of metal solidification process: II—experimental setup and results, *Int. J. Heat Mass Transfer*, **42** (1999), pp. 2129–2142.

[10] R. C. Sun, Simulation and study of surface conductance for heat flow in the early stage of casting, *AFS Cast Metals Research Journal*, **6** (1970), pp. 105–110.

[11] T.-G. Kim and Z.-H. Lee, Time-varying heat transfer coefficients between tube-shaped casting and metal mold, *Int. J. Heat Mass Transfer*, **40** (1997), pp. 3515–3525.

[12] O. Ehrich, Y.-K. Chuang, and K. Schwerdtfeger, The melting of sponge iron spheres in their own melt, *Arch. Eisenhüttenwesen*, **50** (1979), p. 329.

[13] Q. Jiao and N. J. Themelis, Mathematical modelling of heat transfer during the melting of solid particles in liquid slag or melt bath, *Canadian Metallurgical Quarterly*, **32** (1993), pp. 75–83.

[14] F. A. Mucciardi, *A study of light alloy addition techniques in steelmaking*, Ph.D. thesis, McGill University, Canada, 1980.

[15] E. Røhmen, T. Bergstrøm, and T. A. Engh, Thermal behaviour of a spherical addition to molten metals, in *INFACON 7*, Eds.: Tuset, Tveit, and Page, FFF, Trondheim, Norway, 1995, pp. 683–695.

[16] N. J. Goudie and S. A. Argyropoulos, Technique for the estimation of thermal resistance at solid metal interfaces formed during solidification and melting, *Canadian Metallurgical Quarterly*, **34** (1995), pp. 73–84.

[17] S. Farner, *Continuous remelting of aluminium scrap*, Dr.Ing. thesis to be published in 2000, Norwegian Univ. of Science and Technology, Trondheim, Norway.